JCTC Journal of Chemical Theory and Computation

Article

pubs.acs.org/JCTC

Two Dimensional Epitaxial Water Adlayer on Mica with Graphene Coating: An *ab Initio* Molecular Dynamics Study

Hui Li and Xiao Cheng Zeng*

Department of Chemistry and Nebraska Center for Materials and Nanoscience, University of Nebraska—Lincoln, Lincoln, Nebraska 68588, United States

Supporting Information

ABSTRACT: Motivated by a recent atomic-force-microscopy (AFM) study of water adlayers on mica by Heath and co-workers (Graphene Visualizes the First Water Adlayers on Mica at Ambient Conditions. *Science* **2010**, *329*, 1188), we performed an *ab initio* molecular dynamics study of structural and dynamic properties of monolayer, bilayer, and trilayer water adlayers on the muscovite mica (001) surface with and without a graphene coating. We find that in the first epitaxial water adlayer, water molecules that form strong hydrogen bonds with the oxygen on the mica surface show little motions, thereby solid-like, while those "bridging" water molecules on top of the first water adlayer exhibit "itinerant" behavior, thereby liquid-like. Overall, the Born−Oppenheim molecular dynamics (BOMD) simulations (based on the BLYP-D functional) show that the first water adlayer on mica exhibits a unique hybrid solid−liquid-like behavior with a very low diffusion coefficient at ambient conditions. In particular, no dangling hydrogen bonds are found in the first water adlayer on mica. Moreover, the bilayer and trilayer water adlayers show slightly higher structural stability than the first water adlayer. A graphene coating on the water adlayer further enhances stability of the water adlayers. Most importantly, the bilayer water adlayer on mica with the graphene coating becomes fully solid-like, the structure of which is the same as the bilayer slice of ice-I_h with a thickness of 7.4 Å, consistent with the AFM measurement.

I. INTRODUCTION

Understanding properties of a thin film of water adsorbed on a solid surface has important implications in many physical processes,[1] such as changing chemical reactivity of salt particles upon the evaporation of seawater,[2] cloud formation on aerosol particles,[3] transformation of solid phases,[4] mineral weathering, and alteration of soil properties.[5] A deeper insight into the molecular structure of vicinal water is critical to understanding properties of the water adlayer on a solid. Over the past two decades, the topic of surface induced ice formation under ambient conditions has received increasing attention from surface scientists.[1,6] Numerous surface-induced ice structures have been observed on either metal or insulator surfaces, such as Pt (111),[7] Cu (110),[8] MgO (100),[9] and NaCl (100) surfaces,[10] among others. Theoretical chemists and physicists have also attempted to predict new quasi-two-dimensional (2D) ice structures on solid surfaces. For example, bilayer hexagonal, monolayer square, or square-octagonal 2D ice structures have been predicted to form near ambient temperature and within hydrophobic slit nanopores in previous classical molecular dynamics (MD) simulations.[11,12] Later, the existence of bilayer hexagonal ice was confirmed experimentally with water molecules being deposited on a graphene surface between 100 and 140 K.[13] This bilayer hexagonal ice consists of two parallel hexagonal sheets, one being stacked on top of the other, which is structurally different from the hexagonal bilayer slice of 3D I_h-ice.

Muscovite mica is widely used as a hydrophilic substrate in the study of properties of vicinal water. Due to a close match between the lattice constant of the water adlayer and the underlying mica substrate, the mica surface can serve as a nucleating agent to induce 2D water−ice phase transition.[14−16] The water adlayer on mica typically exhibits a structure close to the crystalline form of ice (see Figure 1A and B), as predicted by Odelius et al.[17] from quantum molecular dynamics simulation. Previous scanning polarization force microscopy (SPFM) experiments also showed that the edge of the water monolayer on mica has a preponderance of angle of 120°, indicating an ice-like structure.[18,19] The sum frequency generation (SFG) experiment revealed that there are no dangling OH bonds sticking out from the surface of the water adlayer on mica.[20] On the other hand, ellipsometry measurement indicated that water on mica is more fluid-like, especially with increasing water film thickness.[21] All of these experiments demonstrate thickness-dependent water structures on the mica (001) surface. Recently, water adlayers on a (muscovite) mica (001) surface with (or without) a graphene coating under ambient conditions were studied by Heath and co-workers, using AFM.[22] They found that the thicknesses of single and double layers of water between the mica (001) and graphene sheet are the same as that of single and double layers of normal ice (ice I_h), respectively, and the water can epitaxially grow on the mica (001) surface in a strictly layer-by-layer fashion. This sandwich-like mica−water adlayer-graphene system provides an ideal model for the study of the 2D ice/water structure confined to a hydrophobic surface (graphene) and a hydrophilic surface (mica).

There have been several classical MD and Monte Carlo simulations of mica/water interfacial systems reported in the

Received: June 8, 2012
Published: August 14, 2012

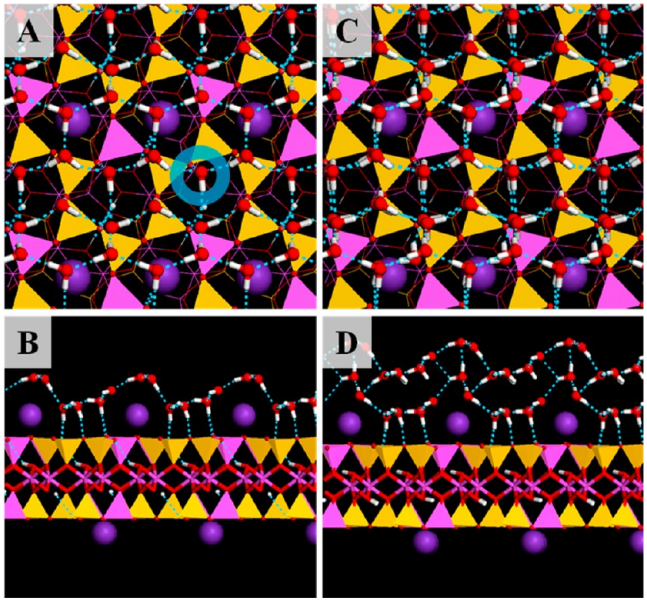

Figure 1. Optimized structures of monolayer and bilayer **Ice-A** on the mica (001) surface (**Sys-I**). A top view of monolayer and bilayer **Ice-A** is shown in A and C, respectively, as well as a side view of monolayer and bilayer **Ice-A** exhibited in B and D, respectively. Color code: O (red), H (white), Al (pink), Si (yellow), K (purple). Blue dashed lines denote hydrogen bonds. The 5-coordinated water molecule is highlighted by a blue circle in A.

literature.[23−26] In these simulation studies, the water−water and water−mica hydrogen bonding interactions were described by empirical potential functions. *Ab initio* methods, such as density-functional theory (DFT), can account for water−mica and water−water interactions more accurately. However, due to high computational cost, previous *ab initio* MD simulations typically employed a relatively small supercell (e.g., 2 unit cells of mica) and short time (∼2 ps), which was insufficient to compute the diffusivity of water molecules in the water adlayer.[17] Also, many previous DFT calculations did not include correction to account for dispersion interaction. Over the past few years, several versions of the dispersion-corrected DFT (DFT-D) method have been developed to better describe the weak intermolecular interaction, such as the dispersion. Certain benchmark calculations based on DFT-D methods for noncovalent systems have been shown to reach the accuracy of coupled-cluster (with modest basis sets) calculations.[27] Here, we employ BOMD simulations based on a DFT-D method to investigate structural properties and diffusivity of epitaxial water adlayers on the mica (001) surface. Toward this end, a relatively large system size and long simulation times (20−30 ps) are used. We note that a problem for construction of the mica/water system in computer simulation is that the positions of K^+ ions on the mica surface are largely unknown. Yet, the presence of charge-balancing K^+ cations on the mica surface can significantly affect the structure of the water adlayer.[23] To dodge this well-known problem, we consider two model systems for the mica (001) surface: one involves K^+ ions, and another does not. More specifically, the first model system initially includes an ice-I_h film on the mica (001) with K^+ ions located between the ice film and the mica surface (**Sys-I**) as used in previous *ab initio* MD simulation.[17] The second model system initially has just an ice-I_h film on an atomically flat mica (001) surface without K^+ ions (**Sys-II**), as observed in the AFM experiment.[22]

In this article, we report an *ab initio* MD study of the melting process of the ice film in both **Sys-I** and **Sys-II** within the temperature range of 250 to 380 K and the structural properties and diffusivity of the water adlayer on mica. In addition, a water (or ice) film between the mica surface without K^+ ions and a graphene sheet is also simulated to study how the hydrophobic coating (graphene) can stabilize the ice film (or water adlayer) on the mica substrate. Both monolayer and multilayer ice/water films are simulated to explore the layer-dependent melting process and structural properties, as well as the link between structural stability and the number of water adlayers. Our BOMD simulations suggest that the ice film in **Sys-I** (named **Ice-A**) is thermodynamically less stable than that in **Sys-II** (named **Ice-B**). Furthermore, the ice film in **Sys-I** cannot form

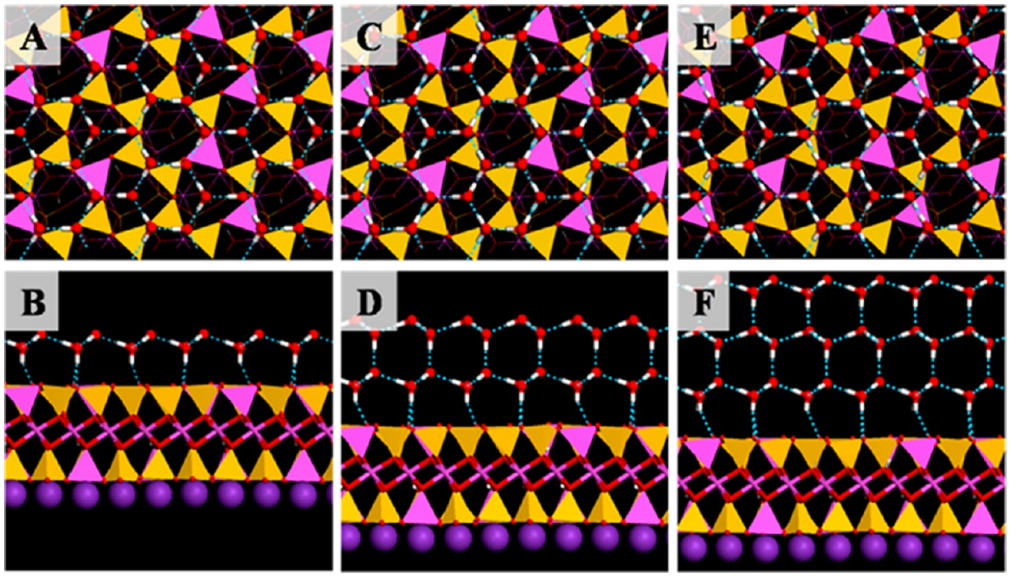

Figure 2. Optimized structures of monolayer and bilayer **Ice-B** on the mica (001) surface (**Sys-II**). A top view of monolayer, bilayer, and trilayer **Ice-B** is shown in A, C, and E, respectively, and a side view of monolayer, bilayer, and trilayer **Ice-B** is displayed in C, D, and F, respectively.

a stable second epitaxial ice layer. Although the monolayer ice film entails low thermal stability, interestingly, its thickness is very close to that of a single layer of ice-I_h. The layer-by-layer growth model for the water adlayer in **Sys-II** is confirmed by the high stability of the second and third water adlayer structures. In particular, we find that the graphene coating can fully stabilize the bilayer **Ice-B** structure.

II. MODELS AND SIMULATION METHODS

The monoclinic crystalline structure of the muscovite mica ($C2/c$ $2M_1$) with chemical formula $KAl_2(Si_3Al)O_{10}(OH)_2$ is chosen as the substrate in the BOMD simulation.[28] The bulk mica consists of negative charged aluminosilicate layers and positive charged K^+ counterions between the layers. The basic structure of the aluminosilicate layer (called the TOT layer) is composed of two separated SiO_4/AlO_4 tetrahedron layers connected by a dioctahedral Al sheet. The SiO_4/AlO_4 layers have an Al/Si ratio of 1:3. The K^+ ions in the bulk mica are all coordinated with the bridging oxygen atoms in the tetrahedron layers. The exact structure of the mica surface is still not fully resolved because the positions of K^+ ions on the mica surface are difficult to determine. It is possible that a fraction of K^+ ions on the mica surface may be replaced by H_3O^+ ions. Some experiments showed that a neutral mica (001) surface may lack surface K^+ ions.[29] In the simulation of **sys-I**, the same model mica (001) surface was used as in a previous *ab initio* MD simulation where the K^+ ions were located at the center sites of six-member rings containing two Al and four Si atoms (see Figure 1). On the other hand, according to the recent AFM experiment,[22] the normal ice-I_h film can only grow on an atomic flat surface in a layer-by-layer fashion. It is possible that in some experimental samples of mica, the redundant K^+ ions may diffuse into the lower intervals of mica, or relocate at some defect positions. Thus, for the simulation of **sys-II**, we employ a clean mica (001) surface model where all K^+ ions are located on the bottom side of the mica layer, as shown in Figure 2. The experimental lattice constants of mica (a: 5.2 Å, b: 9.0 Å)[28] are utilized. The periodic model system has a 3×1 unit cell in the lateral (x−y) dimensions, and a single aluminosilicate layer in the z dimension. Above the mica surface, monolayer and multilayer epitaxial ice structures (**Ice-A** and **Ice-B**) are initially placed, respectively, on the mica surface. The vacuum space in the z direction is about 10 Å. A density functional theory (DFT) method in the form of the Becke−Lee−Yang−Parr (BLYP)[30,31] functional is chosen to compute the potential gradient in the BOMD simulation. The core electrons are described by the Goedecker−Teter−Hutter (GTH) norm-conserving pseudopotential,[32,33] and the basis sets are a combination of the polarized double-ζ quality Gaussian basis[34] and a plane-wave basis set (with an energy cutoff of 280 Ry). Only the Γ point is sampled in the Brillouin zone of the supercell. Note that the DFT/BLYP method within the general gradient approximation (GGA) underestimates the weak dispersion interaction. Hence, we employ the Grimme dispersion corrected DFT-D method[27] to better describe the intermolecular interactions. All of the BOMD simulations are carried out using the QUICKSTEP program implemented in the *CP2K* software package.[35,36] Before BOMD simulations, a geometry optimization of the system is performed with all atomic positions allowed to relax. Thereafter, BOMD simulations are performed in the canonical ensemble. The temperature of the system is increased stepwise from 250 to 380 K to investigate the melting processes in three independent simulations, and to examine thermodynamic stability of 2D ice on mica. The total simulation time for each simulation is 20.0−30.0 ps, with the time step being 1.0 fs. The first 5 ps are for equilibration of the system ,and the remaining run time is used for property calculation.

III. RESULTS AND DISCUSSION

A. Optimized Structures and Average Binding Energies. Optimized structures of **Ice-A** and **Ice-B** are displayed in Figures 1 and 2, respectively. As shown in Figure 1A and B, the monolayer structure of **Ice-A** is similar to a single (puckered) slice of ice-I_h with distorted hexagons in which the OH bonds of water molecules on the lower plane of the puckered slice are connected with other water molecules via intermolecular hydrogen bonds and with the oxygen atoms on the mica. Here, no dangling OH bond exists in **Ice-A**, consistent with the result from the SFG experiment at higher temeratures.[20] We also place the second layer of the **Ice-A** structure with the same initial shape as the first layer. However, as shown in Figure 1D, water molecules in the second layer exhibit many dangling hydrogen bonds, indicating that this bilayer structure is likely unstable at ambient conditions. This explains why the bilayer **Ice-A** structure cannot be maintained in the BOMD simulation even below ambient temperature (see below). For **Sys-II** (without K^+ ions), because lattice constants of ice-I_h are very close to those of the aluminosilicate surface, the monolayer **Ice-B** structure turns out to be the same as a slice of ice-I_h, where those OH bonds pointing to the substrate are bonded with the oxygen atoms on the mica surface. Thus, the second and third ice-I_h like water adlayers could be grown epitaxially on the first layer, as shown in Figure 2D and F. Another significant difference between **Ice-A** and **Ice-B** is that there is one 5-coordinated water molecule per unit cell in the hydrogen bonding network of **Ice-A**, whereas in **Ice-B** every water molecule is either 4-coordinated or 3-coordinated. It is known that water molecules in normal ice are predominately 4-coorinated. Thus, the 5-coordinated water molecule must involve a two-centered hydrogen bond. This feature in coordination number can explain why **Ice-B** is more stable than **Ice-A** in general.

Relative stabilities of **Ice-A** and **Ice-B** structures are also manifested in the computed average binding energy (or cohesive energy) per water molecule (where the effect of mica or graphene is included), as shown in Figure 3. Indeed, **Ice-B** possesses more negative binding energy than **Ice-A**. The binding energy per water molecule for the bilayer **Ice-A** and **Ice-B** is less negative than that of the monolayer ice, indicating that the interaction between the first water adlayer and the mica surface is stronger than the interlayer interaction between the first and second water adlayers. This strong interfacial interaction between the water adlayer and mica is the reason why the water adlayer tends to fully cover the mica surface. Interestingly, the trilayer **Ice-B** has a more negative binding energy than the bilayer **Ice-B** due to the increased long-range interaction. The position of the purple line in Figure 3 represents the cohesive energy of bulk ice-I_h calculated at the same DFT level. It can be seen that both monolayer **Ice-A** and **Ice-B** have less negative binding (or cohesive) energy than the 3D normal ice-I_h. Surprisingly, the binding energies of **Ice-B** systems with a graphene coating (here the average binding energy is computed on the basis of the formula $E_b = [E(\text{mica+water+graphene}) - E(\text{mica+graphene configuration at each snapshot}) - n_w E(\text{isolated water molecule})]/n_w$, where n_w is the

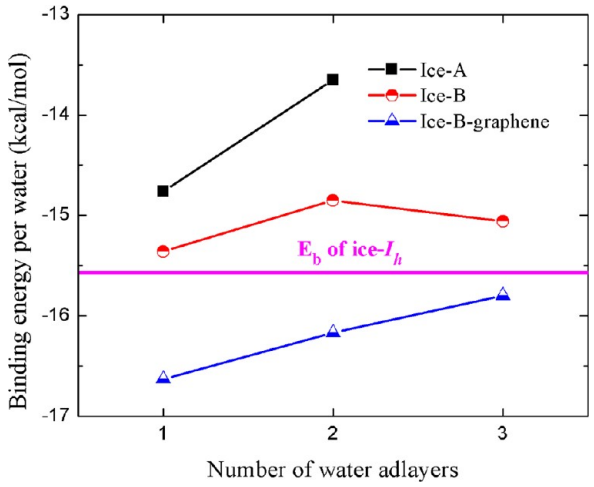

Figure 3. Computed average binding energies per water of **Ice-A**, **Ice-B**, and **Ice-B** coated by a graphene, as well as the computed cohesive energy of the normal ice-I_h (horizontal pink line).

number of water molecules in the system) are actually more negative than that of the normal ice-I_h (see the blue line in Figure 3), implying that the graphene coating will likely enhance stability of the **Ice-B** structure under ambient conditions. Note that the water−graphene interaction (van de Waals type) is short-ranged, which decays rapidly with the distance from the graphene surface. This explains why the average binding energy of trilayer **Ice-B** is less negative than that of bilayer **Ice-B** with the presence of graphene coating. Overall, with increasing of the number of water layers, the binding energies of **Ice-B** and **Ice-B**/graphene are closer to the bulk ice-I_h, as shown in Figure 3. The small binding energy (in magnitude) of the bilayer **Ice-A** implies a likelihood of instability for the multilayer **Ice-A** form under ambient conditions.

B. Melting Behavior of Ice-A and Ice-B. First, we perform BOMD simulations of the melting of the monolayer **Ice-A** as the temperature is raised stepwise from 250 K to 300 K, 340 K, and 380 K (see Figure 4). In this case, K^+ ions appear to be quite stable above the center of the Si−Al−O six member rings of the mica (001) surface without showing significant movement in the BOMD simulations. This result is consistent with previous classic MD simulations. The **Ice-A** monolayer maintains a solid-like structure at 250 K during 30 ps simulation, as shown in Figure 4A. In particular, the water molecules bonded to the oxygen atoms on mica retain their initial positions and orientations. However, the upper bridging water molecules of **Ice-A** around the K^+ ions show significant displacements and rotations. A small fraction of OH bonds of water molecules that point upward are observed at 250 K. It shows that dangling OH bonds can exist in the **Ice-A** structure even at the relatively low temperature due to the low stability of the bridging water molecules around K^+ ions. This conclusion differs from that from the SFG experiment.[20] When the temperature is increased to 300 K or higher, the monolayer **Ice-A** starts to show melting behavior. However, even though the ice-like hydrogen-bond network collapses, the hydrogen bonds between water molecules and the mica are still unbroken even at temperatures up to 340 K (Figure 4C). Such a strong interfacial interaction can explain why the first water adlayer can be highly stable on the mica (001) surface under ambient conditions, regardless of its state (solid-like or hybrid solid−liquid-like). At 380 K, the interfacial hydrogen bonds are

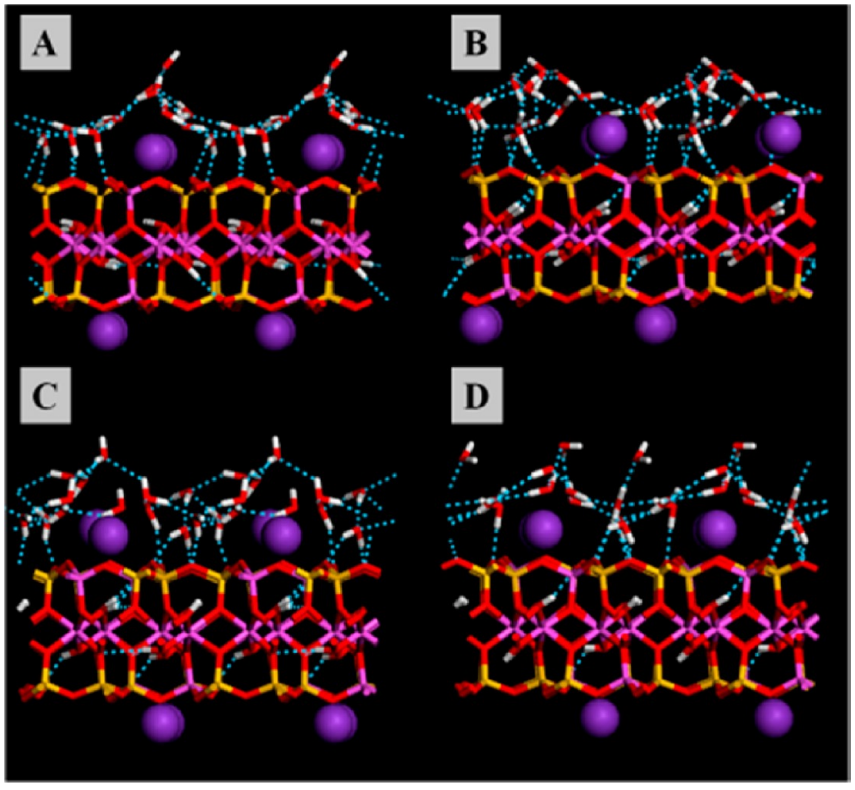

Figure 4. A side view of the final configuration of the monolayer **Ice-A** structure on mica (001) at (A) 250 K, (B) 300 K, (C) 340 K, and (D) 380 K at the end of a 30 ps BOMD simulation, respectively.

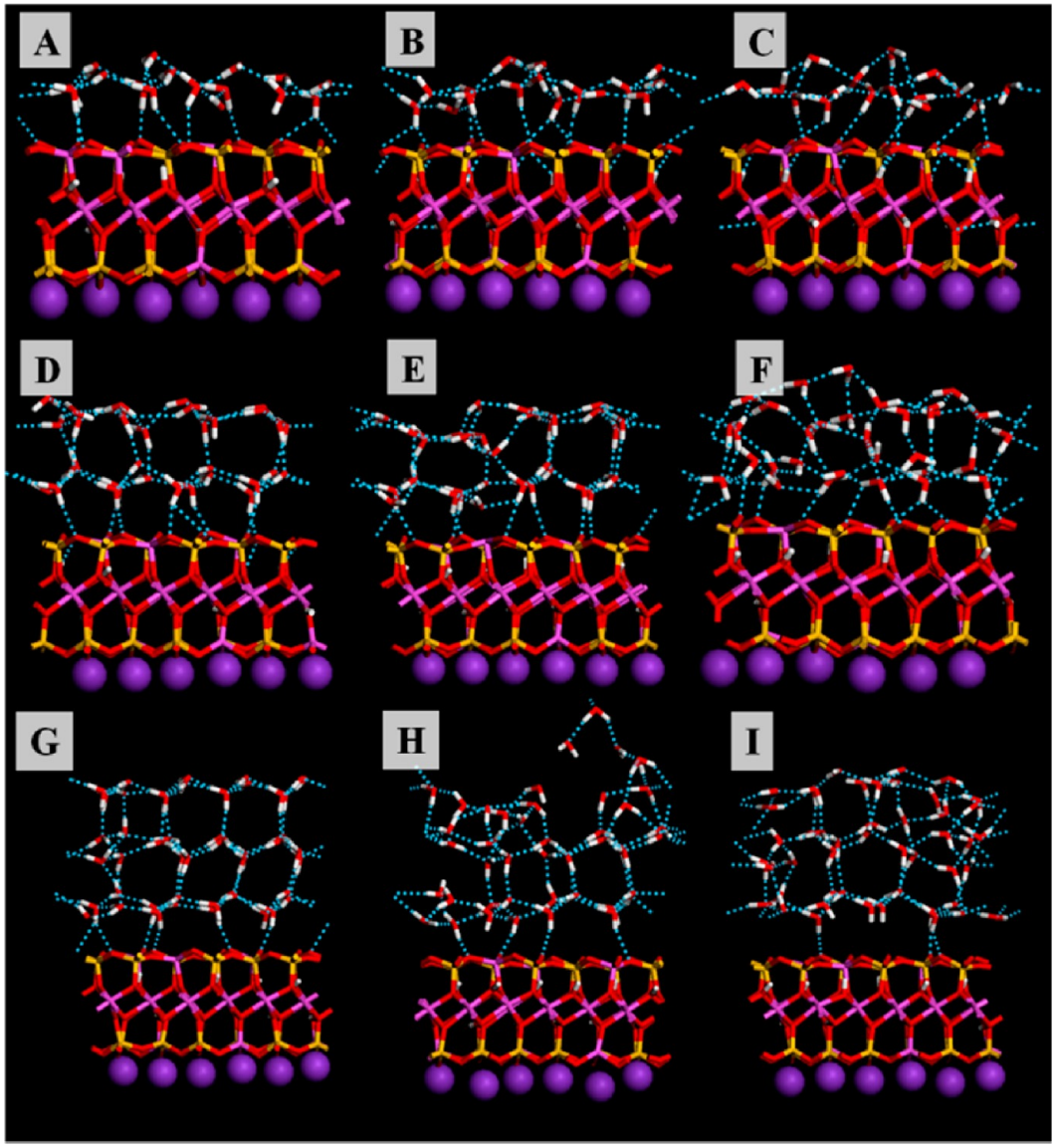

Figure 5. A side view of the final configuration of the monolayer **Ice-B** structure on mica (001) at (A) 250 K, (B) 300 K, and (C) 340 K. A side view of the final configuration of the bilayer **Ice-B** structure at (D) 250 K, (E) 300 K, and (F) 340 K, as well as the final configuration of the trilayer **Ice-B** structure at (G) 300 K, (H) 340 K, and (I) 360 K. The simulation time is 20−25 ps.

broken. A significant number of dangling OH bonds is observed at the higher temperature.

The melting behavior of monolayer **Ice-B** is similar to that of **Ice-A**. At 250 and 300 K, the monolayer **Ice-B** is partially liquid-like, consistent with previous classical MD simulations.[23] Water molecules bonded to the mica are maintained in their initial position, and their orientations are also well kept (see Figure 5A and B). However, those upper bridging water molecules connecting to lower vertically oriented water molecules exhibit much larger displacement, and as such the six-membered rings of **Ice-B** are distorted. This behavior differs from that of **Ice-A**, where a small fraction of dangling OH bonds is observed. At 340 K, the monolayer **Ice-B** is completely liquid-like, where all water molecules exhibit notable diffusion, and the hydrogen bond network is no longer intact. Furthermore, some of water molecules show a tendency to desorb from the mica (Figure 5C).

Compared to the monolayer, the bilayer **Ice-B** appears to be more stable on the mica (001) surface. The bilayer **Ice-B** is still solid-like at 250 K as shown in Figure 5D. At 300 K, the structure of double-slice ice-I_h is largely maintained, although a small deformation can be observed at the end of the MD simulation (25 ps), as shown in Figure 5E. This suggests that the melting temperature of bilayer **Ice-B** is above but close to 300 K. Nevertheless, no dangling OH bond is found in bilayer **Ice-B** at 300 K. Figure 5F shows that at 340 K, the bilayer **Ice-B** structure collapses and becomes liquid-like. Last, for trilayer **Ice-B**, its structure remains solid-like at 300 K, implying that the additional ice slice enhances the overall stability of the 2D ice. Interestingly, a small number of water molecules in the middle layer of trilayer **Ice-B** can rotate and form hydrogen bonds with the water molecules in the top layer. Note that the rotation of the water molecule has also been investigated in bulk ice and protein systems.[37] Similar to bilayer **Ice-B**, trilayer **Ice-B** exhibits significant melting behavior at 340 and 360 K, as shown in Figure 5H and I, respectively.

We note that some previous experiments, such as AFM[23] and SPFM experiments,[18,19] have shown that monolayer ice on the

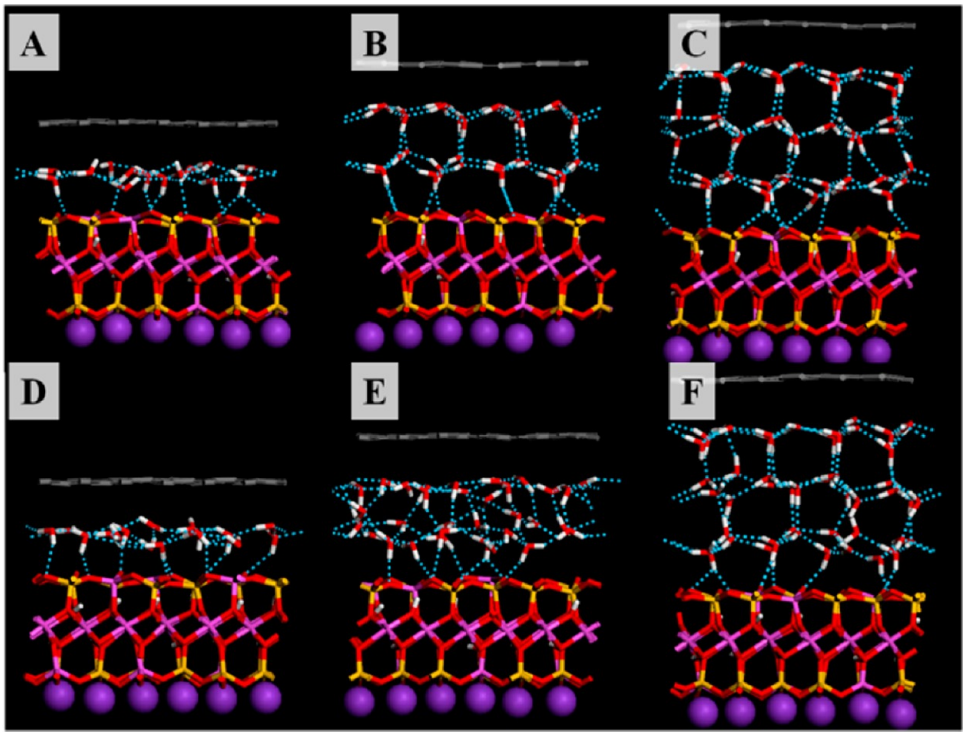

Figure 6. A side view of the final configuration (at the end of 20−25 ps simulations) of the monolayer (A), bilayer (B), and trilayer (C) **Ice-B** structure at 300 K and monolayer (D), bilayer (E), and trilayer (F) **Ice-B** at 340 K. The **Ice-B** structure is initially confined between the mica (001) surface and a graphene sheet.

mica (001) surface is very stable. The melting point of this monolayer ice can be even higher than that of the normal ice-I_h. However, our BOMD simulation suggests that the normal ice has a higher melting point[38,39] than monolayer **Ice-B** on mica (001). A possible reason for the difference is that in our simulation system, only a single layer of mica is included due to a limitation of computational resources, whereas the mica substrate used in the laboratory experiments is considerably thicker. The realistic mica surface should have stronger interaction with water molecules, which renders the melting point of monolayer ice higher. Indeed, our BOMD simulations of the melting behavior of the monolayer, bilayer, and trilayer of **Ice-B** clearly indicate that the water molecules bonded to mica are in a solid-like state, whereas the bridging water molecules are more likely in a liquid-like state. As a result, the second ice layer can stabilize the first water adlayer, while the trilayer water adlayer is slightly more stable than the bilayer water adlayer. This result is also consistent with the fact that the melting point of finite-sized water increases with the size of the system. On the basis of this trend, it is expected that when the number of water adlayers increase, the melting point of **Ice-B** will approach that of the bulk ice-I_h from below.

We also investigate the melting of **Ice-B** on the mica (001) surface but with a graphene coating on top, as done in the AFM experiment.[22] This sandwich-like system for the water adlayer offers an ideal model system to study the behavior of water/ice confined between a hydrophilic surface (mica) and a hydrophobic (graphene) surface. Final configurations (snapshots) of **Ice-B** structures between the mica and graphene sheet are presented in Figure 6. The physical behavior of monolayer **Ice-B** is almost the same at 300 and 340 K, where it shows hybrid solid−liquid-like behavior (see Figure 6A and D and Supporting Information Movie S1). The water molecules bonded to the mica surface appear to be in a solid-like state while the bridging water molecules are in a liquid-like state. Unlike the monolayer, bilayer **Ice-B** shows marked stability at 300 K with the graphene coating. As shown in Figure 6B and Movie S2, the bilayer **Ice-B** structure is intact without showing significant displacement and rotation of water molecules during the BOMD simulation. In fact, bilayer **Ice-B** remains solid-like at 320 K, indicating that the melting temperature of bilayer **Ice-B** should be higher than 320 K. Figure 6E shows the melting of bilayer **Ice-B** at 340 K. With the graphene coating, trilayer **Ice-B** shows higher stability at 300 K as well (Figure 6C and Movie S3), although events of water molecule fipping in the middle layer can still be observed. Even at 340 K, the basic structure of trilayer **Ice-B** is still maintained, except some distortions and rotations of the middle layer, which suggests that the melting temperature of trilayer **Ice-B** is close to 340 K. On the other hand, without the graphene coating, trilayer **Ice-B** appears to possess a slightly higher melting temperature than bilayer **Ice-B**. We note that the 2D ice structure beyond the bilayer was not observed in the previous AFM experiment.[22] One possible explanation is that our simulation time (20−30 ps) is too short. For example, the flip of the water molecules observed inside trilayer **Ice-B** may cause instability for a very thin ice film, which can eventually lead to structure collapse on a much longer time scale. In any event, the fact that the melting temperature of **Ice-B** with a graphene coating is higher than that without the graphene coating shows that the graphene coating can significantly enhance the stability of the water adlayer on mica.

C. Angle and Density Distributions. To further investigate detailed interfacial structures of the ice/water adlayer on mica, the distribution of the angle (ω) between the z axis (normal to the mica surface) and the OH bonds of

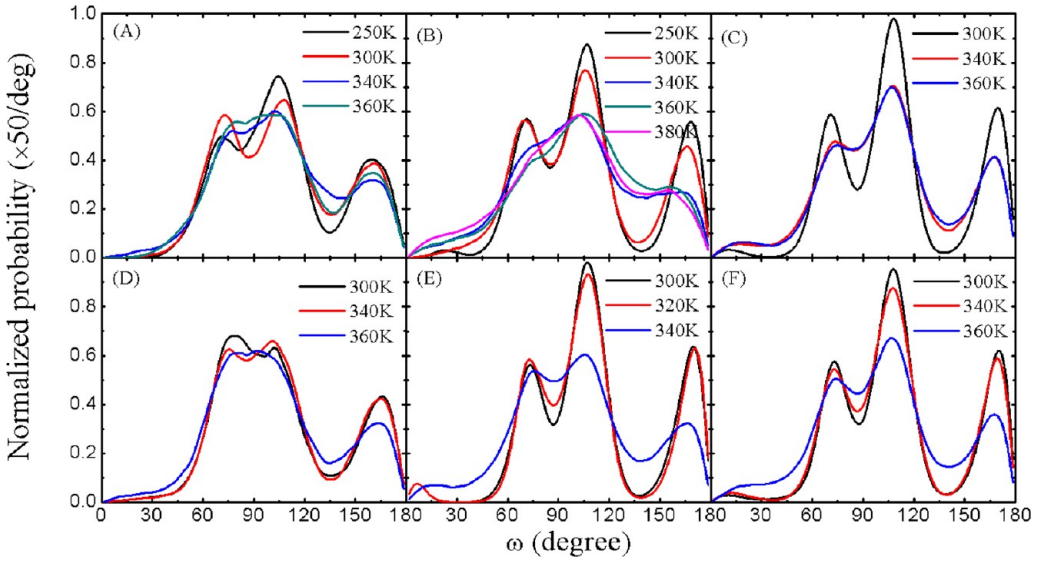

Figure 7. Distributions of the angle (ω) between the z axis (normal to the mica surface) and the OH bonds of water molecules in the (A) monolayer, (B) bilayer, and (C) trilayer of the **Ice-B** structure, as well as the (D) monolayer, (E) bilayer, and (F) trilayer of the **Ice-B** structure with a graphene coating and at various temperatures.

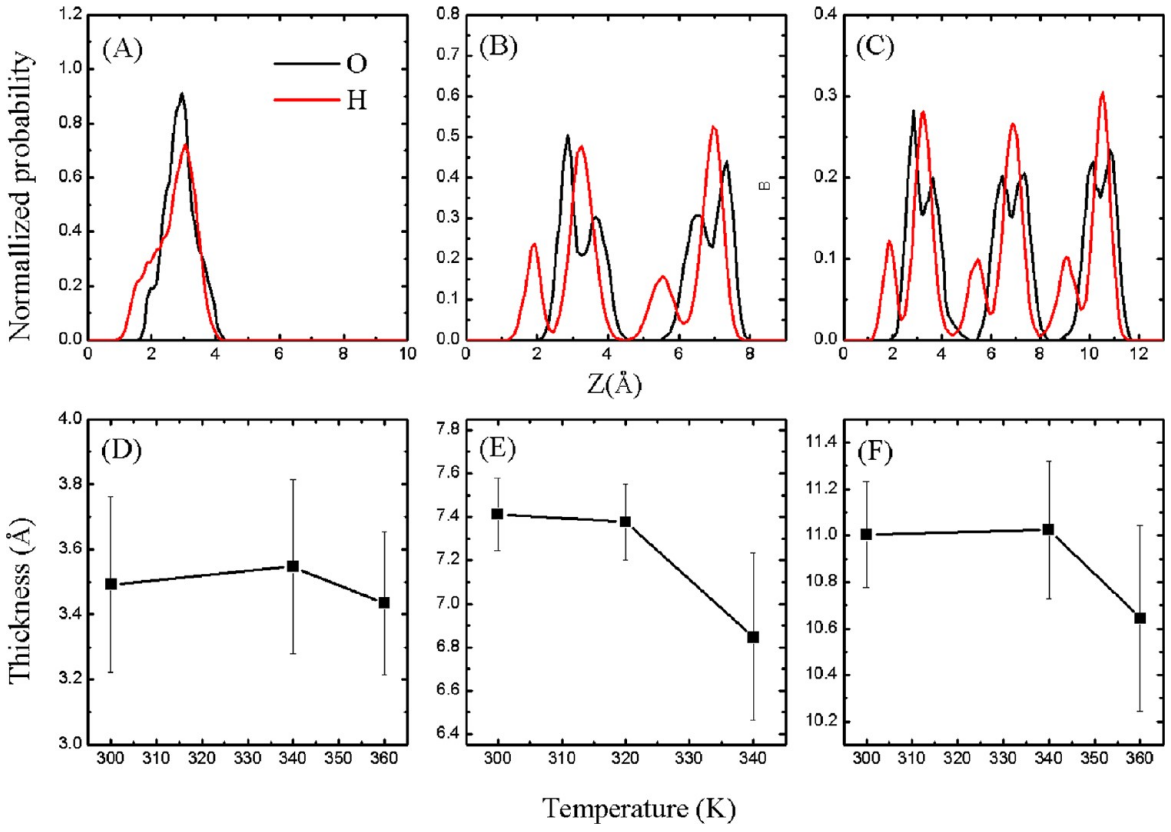

Figure 8. Density profiles of oxygen and hydrogen of water at 300 K along the z axis for the (A) monolayer, (B) bilayer, and (C) trilayer of the **Ice-B** structure with a graphene coating. The average thickness of the (D) monolayer, (E) bilayer, and (F) trilayer of the **Ice-B** structure with the graphene coating at various temperatures.

water molecules in **Sys-I** and **Sys-II** is computed (see Figures S1 and 7, respectively). Three major peaks can be seen in the distribution of ω in all systems at relatively low temperatures. The peaks at 165° and 75° correspond to water molecules with one OH bond pointing toward the mica and another OH bond pointing slightly upward, while the peak around 105° corresponds to the water molecules having both OH bonds pointing slightly toward to mica surface. The area underneath the peak at 105° is nearly the same as the sum of areas underneath the other two peaks. The three major peaks become wider and lower with an increase of the temperature due to the increasing disorder in the orientation of water molecules. The dangling OH bonds pointing upward and the flip of the water molecules result in a nonzero distribution close

dx.doi.org/10.1021/ct300476f | J. Chem. Theory Comput. 2012, 8, 3034−3043

to 0°. For monolayer **Ice-A**, the probability distribution for $\omega <$ 30° is much higher than that for monolayer **Ice-B** at all temperatures, indicating the existence of much more dangling OH bonds in **Ice-A**. In the distribution curves for monolayer **Ice-B** with no or a graphene coating (Figure 7A and D), the middle peak at 105° is wider and lower than those for bilayer and trilayer **Ice-B**, due to the higher diffusivity of the bridging water molecules not bonded to mica. No peak is seen below 30° in the ω distribution, indicating the nonexistence of a dangling OH bond in monolayer **Ice-B**. In the OH angle distribution of bilayer **ice-B** at 250 and 300 K (Figure 7B), the three major peaks are well separated, while the peaks are much more broadened above 300 K due to increased melting events. For example, a clear phase transition can be identified between 320 and 340 K for bilayer **Ice-B** with a graphene coating (Figure 7E). Such a transition also occurs between 300 and 340 K for trilayer **Ice-B** without a graphene coating (Figure 7C), and between 340 and 360 K with a graphene coating (Figure 7F). However, a minor peak close to 0° arises in the angle distribution for all of the bilayer and trilayer water adlayers, except bilayer **Ice-B** with a graphene coating. This result indicates that the flip of water molecules does not occur in bilayer **Ice-B** with a graphene coating, which again supports bilayer **Ice-B** with a graphene coating being highly stable under ambient conditions.

The bilayer ice-like structures with a graphene coating can also be analyzed via computing the density profiles of oxygen and hydrogen atoms of water in the normal direction (along the z axis), as displayed in Figure 8. The distributions of O and H atoms for bilayer (Figure 8B) and trilayer (Figure 8C) **Ice-B** at 300 K exhibit separated peaks, indicating that the water molecules exhibit high position order. The distance between the adjacent highest peaks of O atoms is about 3.7 Å, the same as the thickness of a single slice of ice-I_h, as measured in the AFM experiment.[22] However, no separated peaks can be observed in the oxygen and hydrogen profiles of the monolayer, suggesting that the structure of the monolayer water adlayer on the mica (001) surface is not fully ice-like at 300 K. To compare with the AFM experiment, we also calculate the average thicknesses of the monolayer, bilayer, and trilayer water adlayers between mica and graphene sheets at various temperatures. The slight variation in the thicknesses of monolayer, bilayer, and trilayer water are shown in Figure 8D, E, and F, respectively. The average thickness of monolayer **Ice-B** is about 3.5 Å at 300 K and 3.6 Å at 340 K, very close to the measured thickness of 3.7 Å in the AFM experiment,[22] rather than 2.0 Å in the ellipsometry experiment.[40] The 3.5−3.6 Å thickness is largely caused by the vertical water molecules bonded to the mica surface. When the temperature increases to 360 K, the thickness of monolayer water decreases slightly due to the breaking of hydrogen bonds between water molecules and mica. The thicknesses of bilayer and trilayer water adlayers with a graphene coating are 7.4 Å and 11.0 Å, respectively, exactly the same as the thicknesses of double and triple slices of ice-I_h. Moreover, a significant reduction in the thickness caused by melting of the ice structure can be seen in the bilayer water adlayer when the temperature is increased from 320 to 340 K. A similar phenomenon can be observed for the trilayer water adlayer between 340 and 360 K.

D. Dynamic Properties. Vibration spectra of the surface water adlayers with either the **Ice-A** or **Ice-B** structure at 300 K are computed from the Fourier transform of the velocity−velocity autocorrelation functions, as shown in Figure 9. In all

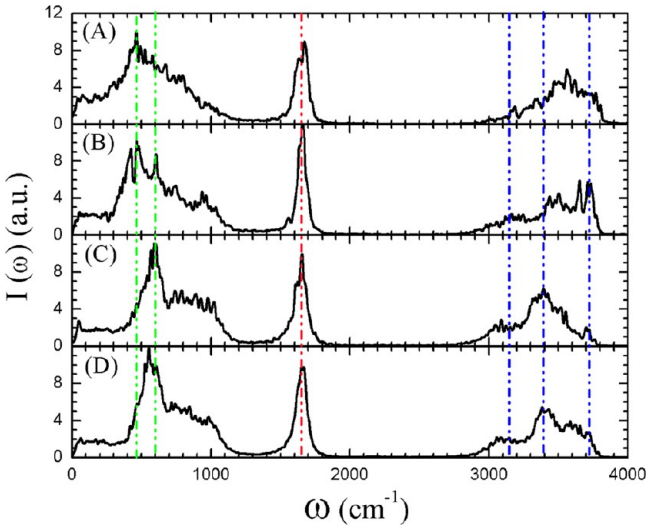

Figure 9. Calculated vibration spectra of water molecules in the (A) monolayer **Ice-A** structure and the (B) monolayer, (C) bilayer, and (D) trilayer **Ice-B** structure at 300 K, based on Fourier transformation of the velocity autocorrelation function of the water adlayer.

spectra, the peak at 1650 cm^{-1} corresponds to the H−O−H angle bending vibration, which does not change with different adlayers. The most important feature in the vibration spectra is the peak at 3700 cm^{-1}, which corresponds to the splitting of the symmetric and antisymmetric components of the OH stretching mode and reflects a change of the stretching frequency from the gas-phase value. The strength of this vibration mode exhibits a dramatic change from monolayer to trilayer water adlayers. In Figure 9A and B, it can be seen that the peak at 3700 cm^{-1} is distinct in the monolayer water adlayer, due to the appearance of dangling OH bonds of the bridging water molecules. This peak vanishes in the vibration spectrum of the bilayer water adlayer (Figure 9C) but arises again in the trilayer water adlayers (Figure 9D), implying that the water molecules in the top layer have a strong tendency to flip and form dangling OH bonds in the trilayer than in the bilayer system. It is interesting that in the SFG vibrational spectroscopy measurement of the D_2O adlayer on mica, it has been observed that the peak of the free OD bond stretching vibration mode goes through the appearance−disappearance−appearance process with an increase in humility.[20] The region of the vibration spectra below 1200 cm^{-1} corresponds to the vibration mode of intermolecular hydrogen bonds. The first highest peak in that region exhibits a blue shift from the monolayer to the bilayer and to the trilayer water adlayer, indicating that the intermolecular hydrogen bonds are stronger in the bilayer and trilayer water adlayer than in the monolayer water adlayer.

On the basis of the BOMD trajectories, the self-diffusion coefficient of oxygen atoms of the water molecules for the **Ice-A**, **Ice-B**, and **Ice-B** structures with a graphene coating at various temperatures are computed on the basis of the mean square displacement (MSD) (see Figures S2 and S3 in Supporting Information) and the Einstein relation. Because the BOMD simulation time is typically on the order of a few tens of picoseconds, which is too short to predict an accurate diffusion coefficient for a solid, only diffusion coefficients of water adlayers with partially liquid-like behavior are computed quantitatively. In other cases, the diffusion coefficient is only estimated qualitatively to analyze dynamic properties of the

Table 1. Computed Diffusion Coefficient (in the unit of cm^2/s) of Oxygen Atoms of the Water Molecules of the Monolayer (ML), Bilayer (BL), and Trilayer (TL) Ice-A Structure, Ice-B Structure, and Ice-B with a Graphene (Gr) Coating at Various Temperatures, Respectively

	ML Ice-A	ML Ice-B	BL Ice-B	TL Ice-B	ML Ice-B-Gr	BL Ice-B-Gr	TL Ice-B-Gr
250 K	8.16×10^{-7}	1.33×10^{-6}	3.14×10^{-7}				
300 K	2.52×10^{-6}	1.60×10^{-6}	8.27×10^{-7}	3.08×10^{-7}	2.88×10^{-6}	~0	4.64×10^{-7}
320 K						~0	
340 K	9.24×10^{-6}	8.33×10^{-6}	5.87×10^{-6}	8.19×10^{-6}	3.97×10^{-6}	1.0×10^{-5}	5.14×10^{-7}
360 K		1.09×10^{-5}	1.50×10^{-5}		9.49×10^{-6}		1.06×10^{-5}
380 K	1.31×10^{-5}		2.57×10^{-5}				

water adlayer on mica. If the MSD curve does not show an obvious slope, the diffusion coefficient is regarded as negligible (or zero), and the corresponding structure is considered to be solid-like. The trajectories after 5 ps are used to compute the MSD, and diffusion coefficients are listed in Table 1. According to the calculated self-diffusion coefficients, two systems are considered to be solid-like, namely, bilayer **Ice-B** with a graphene coating at 300 and 320 K. Interestingly, although diffusion coefficients of trilayer **Ice-B** at 300 K and trilayer **Ice-B** with a graphene coating at 300 and 340 K are much smaller than the diffusion coefficient of bulk liquid water ($\sim 1.2 \times 10^{-5}$ cm^2/s), a notable slope for the oscillatory MSD curves is seen (Figure S3F in Supporting Information), implying that these structures tend to melt slowly in the BOMD simulations. This result also supports a conclusion from the AFM experiment that no ice structure can be observed beyond the bilayer water. The bilayer **Ice-B** at 250 K also possesses a very small diffusion coefficient, but it is not as small as that of a real solid. Furthermore, the monolayer **Ice-A** and **Ice-B** possess comparable diffusion constants, and their diffusion rate is similar to typical supercooled liquid water. In summary, bilayer **Ice-B** with a graphene coating is fully solid-like under ambient conditions.

IV. CONCLUSION

In conclusion, we employ the BOMD simulation method to study the epitaxially grown monolayer, bilayer, and trilayer water adlayers on the mica (001) surface. We consider three possible situations: water adlayers on mica with K^+ ions, water adlayers on mica without K^+ ions, and a sandwich configuration with water adlayers located between a mica (001) surface and a graphene sheet. It is found that water on mica (001) with K^+ ions cannot form a stable epitaxial second adlayer. However, water can form very stable second and third adlayers on the K^+ free mica surface. Computed cohesive energies show that water molecules prefer to form a fully covered monolayer water adlayer on mica due to the strong interfacial interaction between water and the mica surface. Importantly, the monolayer water adlayer behaves neither fully solid-like nor liquid-like under ambient conditions. Instead, it exhibits hybrid solid–liquid-like behavior where the bridging water molecules are itinerary while the water molecules in direct contact with mica are anchored by the oxygen atoms on the mica surface. The bilayer and trilayer water adlayers show higher stabilities than the monolayer adlayer. However, the possibility of flipping water molecules is much higher in the trilayer adlayer than in the bilayer adlayer, rendering the trilayer adlayer structurally less stable. Most importantly, we find that the graphene coating can significantly enhance the stability of the water adlayer in general and render the bilayer water adlayer fully ice-like in particular.

As discussed above, the monolayer water adlayer exhibits hybrid solid–liquid-like behavior because the hydrogen bonding to the oxygen on mica makes the orientation of a large number of water molecules normal to the mica surface. As a result, the average thickness of the monolayer is 3.5–3.6 Å, very close the AFM measurement of 3.7 Å. Furthermore, the self-diffusion coefficient of the monolayer water adlayer is an order of magnitude smaller than that of bulk water. The calculated vibration spectra show a peak of the free OH bonds stretching mode, which is distinctive in the monolayer and trilayer water adlayer but extremely weak in the bilayer water adlayer. Previous SFG experiments also demonstrate a similar feature with an increase in humility of D_2O on mica. The computed diffusion coefficient of water for the bilayer water adlayer with a graphene coating is several orders of magnitude smaller than that of bulk water, indicating that the bilayer water adlayer on the mica (001) surface is indeed ice-like under ambient conditions. These simulation results yield new insights into the physical behavior of the water adlayer on mica with or without a hydrophobic coating.

■ ASSOCIATED CONTENT

Ⓢ Supporting Information

Movies of water adlayers on mica with a graphene coating, computed MSDs, and distributions of angle ω are collected. This material is available free of charge via the Internet at http://pubs.acs.org.

■ AUTHOR INFORMATION

Corresponding Author

*E-mail: xzeng1@unl.edu.

Notes

The authors declare no competing financial interest.

■ ACKNOWLEDGMENTS

This work was supported by grants from the NSF (CBET-1036171 and CBET-1066947) and ARL (W911NF1020099).

■ REFERENCES

(1) Ewing, G. E. Ambient Thin Film Water on Insulator Surfaces. *Chem. Rev.* **2006**, *106*, 1511–1526.

(2) Warneck, P. *Chemistry of the Natural Atmosphere*; Academic Press: San Diego, CA, 1988.

(3) Pruppacher, H. R.; Klett, J. D. *Microphysics of Clouds and Precipitation*; Kluwer Academic Publishers: Dordrecht, The Netherlands, 1997.

(4) Tardos, G. I.; Nicolaescu, I. V.; Ahtchi-Ali, B. Ingress of Atmospheric Moisture into Bulk, Packed Powders. *Powder Handl. Process.* **1996**, *8*, 7–16.

(5) Stumm, W.; Sigg, L.; Sulzberger, B. *Chemistry of the Solid-Water Interface: Processes at the Mineral-Water and Particle-Water Interface in Natural Systems*; Wiley: New York, 1992.

(6) Verdaguer, A.; Sacha, G. M.; Bluhm, H.; Salmeron, M. Molecular Structure of Water at Interfaces: Wetting at the Nanometer Scale. *Chem. Rev.* **2006**, *106*, 1478−1510.
(7) Cerdá, J.; Michaelides, A.; Bocquet, M. L.; Feibelman, P. J.; Mitsui, T.; Rose, M.; Fomin, E.; Salmeron, M. Novel Water Overlayer Growth on Pd(111) Characterized with Scanning Tunneling Microscopy and Density Functional Theory. *Phys. Rev. Lett.* **2004**, *93*, 116101.
(8) Carrasco, J.; Michaelides, A.; Forster, M.; Haq, S.; Raval, R.; Hodgson, A. A One-Dimensional Ice Structure Built from Pentagons. *Nat. Mater.* **2009**, *8*, 427−431.
(9) Picaud, S.; Hoang, P. N. M.; Girardet, C. Geometry of $(NH_3)_n$ and $(H_2O)_n$ Aggregates Adsorbed on Well Characterized MgO(100) and Si(111)-(1 × 1)H Substrates. *Surf. Sci.* **1992**, *278*, 339−352.
(10) Bruch, L. W.; Glebov, A.; Toennies, J. P.; Weiss, H. A Helium Atom Scattering Study of Water Adsorption on the NaCl(100) Single Crystal Surface. *J. Chem. Phys.* **1995**, *103*, 5109−5120.
(11) Koga, K.; Zeng, X. C.; Tanaka, H. Freezing of Confined Water: A Bilayer Ice Phase in Hydrophobic Nanopores. *Phys. Rev. Lett.* **1997**, *79*, 5262−5264.
(12) Bai, J.; Angell, A.; Zeng, X. C. Guest-Free Monolayer Clathrate: Coexistence and Phase Transition between Two-Dimensional Low-Density and High-Density Ice. *Proc. Natl. Acad. Sci. U.S.A.* **2010**, *107*, 5718−5722.
(13) Kimmel, G. A.; Matthiesen, J.; Baer, M.; Mundy, C. J.; Petrik, N. G.; Smith, R. S.; Dohnalek, Z.; Kay, B. D. No Confinement Needed: Observation of a Metastable Hydrophobic Wetting Two-Layer Ice on Graphene. *J. Am. Chem. Soc.* **2009**, *131*, 12838−12844.
(14) Turnbull, D.; Vonnegut, B. Nucleation Catalysis. *Ind. Eng. Chem.* **1952**, *44*, 1292−1298.
(15) Jaffray, J.; Montmory, R. Épitaxies de la glace sur l'iodure d'argent. *C. R. Acad. Sci. (Paris)* **1957**, *245*, 2221.
(16) Bryant, G.; Hallett, J.; Mason, B. The Epitaxial Growth of Ice on Single-Crystalline Substrates. *J. Phys. Chem. Solids* **1959**, *12*, 189−195.
(17) Odelius, M.; Bernasconi, M.; Parrinello, M. Two Dimensional Ice Adsorbed on Mica Surface. *Phys. Rev. Lett.* **1997**, *78*, 2855−2858.
(18) Hu, J.; Xiao, X. D.; Ogletree, D. F.; Salmeron, M. Imaging the Condensation and Evaporation of Molecularly Thin Films of Water with Nanometer Resolution. *Science* **1995**, *268*, 267−269.
(19) Salmeron, M.; Xu, L.; Hu, J.; Dai, Q. High-Resolution Imaging of Liquid Structures: Wetting and Capillary Phenomena at the Nanometer Scale. *Mater. Res. Soc. Bull.* **1997**, *22*, 36−41.
(20) Miranda, P. B.; Xu, L.; Shen, Y. R.; Salmeron, M. Icelike Water Monolayer Adsorbed on Mica at Room Temperature. *Phys. Rev. Lett.* **1998**, *81*, 5876−5879.
(21) Beaglehole, D.; Radlinska, E. Z.; Ninham, B. W.; Christenson, H. K. Inadequacy of Lifshitz Theory for Thin Liquid Films. *Phys. Rev. Lett.* **1991**, *66*, 2084−2087.
(22) Xu, K.; Cao, P.; Heath, J. R. Graphene Visualizes the First Water Adlayers on Mica at Ambient Conditions. *Science* **2010**, *329*, 1188−1191.
(23) Wang, J.; Kalinichev, A. G.; Kirkpatrick, R. J.; Cygan, R. T. The Chemistry of Water on Alumina Surfaces: Reaction Dynamics from First Principles. *J. Phys. Chem. B* **2005**, *109*, 15893−15905.
(24) Park, S. H.; Sposito, G. Structure of Water Adsorbed on a Mica Surface. *Phys. Rev. Lett.* **2002**, *89*, 085501.
(25) Leng, Y.; Cummings, P. T. Hydration Structure of Water Confined between Mica Surfaces. *J. Chem. Phys.* **2006**, *124*, 074711.
(26) Leng, Y.; Cummings, P. T. Fluidity of Hydration Layers Nanoconfined between Mica Surfaces. *Phys. Rev. Lett.* **2005**, *94*, 026101.
(27) Grimme., S. Semiempirical GGA-Type Density Functional Constructed with a Long-Range Dispersion Correction. *J. Comput. Chem.* **2006**, *27*, 1787−1799.
(28) Kuwahara, Y. Muscovite surface structure imaged by fluid contact mode AFM. *Phys. Chem. Miner.* **1999**, *26*, 198−205.
(29) Cheng, L.; Fenter, P.; Nagy, K. L.; Schlegel, M. L.; Sturchio, N. C. Molecular-Scale Density Oscillations in Water Adjacent to a Mica Surface. *Phys. Rev. Lett.* **2001**, *87*, 156103.
(30) Becke, A. D. Density-Functional Exchange-Energy Approximation with Correct Asymptotic Behavior. *Phys. Rev. A* **1988**, *38*, 3098−3100.
(31) Lee, C.; Yang, W.; Parr, R. G. Development of the Colle-Salvetti Correlation-Energy Formula into a Functional of the Electron Density. *Phys. Rev. B* **1988**, *37*, 785.
(32) Goedecker, S.; Teter, M.; Hutter, J. Separable Dual-Space Gaussian Pseudopotentials. *Phys. Rev. B: Condens. Matter.* **1996**, *54*, 1703−1710.
(33) Hartwigsen, C.; Goedecker, S.; Hutter, J. Relativistic Separable Dual-Space Gaussian Pseudopotentials from H to Rn. *Phys. Rev. B: Condens. Matter.* **1998**, *58*, 3641−3662.
(34) VandeVondele, J.; Hutter, J. Gaussian Basis sets for Accurate Calculations on Molecular Systems in Gas and Condensed Phases. *J. Chem. Phys.* **2007**, *127*, 114105−114109.
(35) VandeVondele, J.; Krack, M.; Mohamed, F.; Parrinello, M.; Chassaing, T.; Hutter, J. Quickstep: Fast and Accurate Density Functional Calculations Using a Mixed Gaussian and Plane Waves Approach. *Comput. Phys. Commun.* **2005**, *167*, 103−128.
(36) Lippert, G.; Hutter, J.; Parrinello, M. A Hybrid Gaussian and Plane Wave Density Functional Scheme. *Mol. Phys.* **1997**, *92*, 477−488.
(37) Fischer, S.; Verma, C. S.; Hubbard, R. E. Rotation of Structural Water inside a Protein: Calculation of the Rate and Vibrational Entropy of Activation. *J. Phys. Chem. B* **1998**, *102*, 1797−1805.
(38) Yoo, S.; Zeng, X. C.; Xantheas, S. S. On the Phase Diagram of Water with Density Functional Theory Potentials: The Melting Temperature of Ice I_h with the Perdew-Burke-Ernzerhof and Becke-Lee-Yang-Parr Functionals. *J. Chem. Phys.* **2009**, *130*, 221102.
(39) Yoo, S.; Xantheas, S. S. Communication: The Effect of Dispersion Corrections on the Melting Temperature of Liquid Water. *J. Chem. Phys.* **2011**, *134*, 121105.
(40) Beaglehole, D.; Christenson, H. K. Vapor Adsorption on Mica and Silicon: Entropy Effects, Layering, and Surface Forces. *J. Phys. Chem.* **1992**, *96*, 3395.